

Ultra-highly selective biogas upgrading through porous MXenes

Hector Prats,^a Hannah McAloone,^b Francesc Viñes,^{*a} and Francesc Illas^a

^a *Departament de Ciència de Materials i Química Física & Institut de Química Teòrica i Computacional (IQTCUB), Universitat de Barcelona, c/ Martí i Franquès 1-11, 08028 Barcelona, Spain*

^b *Department of Chemistry, University of Warwick, Coventry, CV4 7AL*

* Corresponding author: francesc.illas@ub.edu

S1. Computational details

Further details of the periodic density functional theory (DFT) calculations follow the discussion in the main text. The valence electron density was expanded in a plane wave basis set with a kinetic cutoff energy of 415 eV. The effect of core electrons on the valence electron density was taken into account through the Projected Augmented Wave (PAW) method,¹ as implemented by Kresse and Joubert.² The Brillouin zone was sampled using a $5 \times 5 \times 1$ \mathbf{k} -point mesh with convergence criterion for electronic updates of 10^{-5} eV, while the relaxation of the atomic positions was allowed until the forces acting on all the relaxed atoms were smaller than 0.01 eV \AA^{-1} . Final total energies were obtained by extrapolation to 0 K (no smearing). Vibrational calculations of the optimized geometries have been by computing the elements of the Hessian matrix as finite differences of 0.03 \AA length. The adsorption energy is calculated from total DFT electronic energies as:

$$E_{ads}^i = E_{i/MXene} - E_{MXene} - E_i \quad (1),$$

Where $E_{i/MXene}$ is the energy of the molecule i adsorbed on the corresponding MXene, E_{MXene} is the energy of the relaxed pristine MXene, and E_i the energy of the isolated molecule i in gas phase. Note that the Zero Point Energy (ZPE) term is included in all reported energy values, which has been calculated within the harmonic approximation as:

$$ZPE = \sum_j^{NMV} \frac{1}{2} h v_j \quad (2),$$

where h is the Planck constant, v_j is the frequency of vibrational mode j , and the summation runs over all vibrational normal modes (NMV). For gas-phase CH_4 and CO_2 , NMV correspond to $3N-6$ and $3N-5$, respectively, where N is the number of atoms. The hindered translator/hindered rotor (HT/HR) model is used for adsorbed CH_4 , and therefore it has $3N-3$ vibrational modes in its adsorbed state. Finally, the harmonic oscillator (HO) model is used for adsorbed CO_2 , leading to $3N$ normal modes of vibration.

In the CH_4 adsorption optimization calculations, between one to three spurious imaginary frequencies remained at the aforementioned convergence level in some cases, yet always smaller than 90 cm^{-1} in magnitude, given the weakly physisorbed nature of the highly stable CH_4 molecule. Additional reoptimizations were carried out for CH_4 adsorption on all the closed-shell systems with a $7 \times 7 \times 1$ \mathbf{k} -point mesh and a tighter convergence criterion of 10^{-7} eV for the electronic updates and forces below $0.003 \text{ eV \AA}^{-1}$. However, subsequent vibrational analysis with 0.003 \AA displacements still showed that spurious imaginary frequencies were observed at this point. Note that these results reinforce the need of using the HT/HR model instead of the HO, as suggested by Sprowl *et al.*³ The

energy barriers for CH₄ translation —*i.e.* diffusion over the surface— and rotation —around an axis perpendicular to the surface— have been estimated through the Climbing-Image Nudged Elastic Band (*CI-NEB*) method,⁴ employing five intermediate images. These images were generated using the atomic simulation environment (*ASE*)⁵ and applying the image dependent pair potential (*IDPP*) procedure.⁶

All M₂C MXene (0001) surface models were taken as previously optimized,⁷ consisting of $p(3\times 3)$ supercells containing 18 metal and 9 C atoms arranged in three atomic layers —*i.e.*, a sandwiched M₂C structure has been used. All MXene layers were allowed to relax during the CH₄ or CO₂ adsorption process. A separating vacuum region of at least 10 Å was inserted to avoid spurious interactions between the periodically repeated slabs.

S2. Parameters used in the HT/HR model

Table S1. Calculated translation (diffusion) energy barriers to a neighboring identical adsorption site, E_b^{trans} and 120° rotation energy barriers around the MXene surface axis, E_b^{rot} , both in eV, for CH₄ physisorbed on the different MXenes on the most stable adsorption mode. These energy barriers are used in the HT/HR model in order to calculate the adsorption free energies.³

MXene	E_b^{trans}	E_b^{rot}
Ti ₂ C	0.13	0.01
Zr ₂ C	0.12	0.01
Hf ₂ C	0.02	0.01
V ₂ C	0.18	0.01
Nb ₂ C	0.20	0.01
Ta ₂ C	0.14	0.01
Cr ₂ C	0.27	0.03
Mo ₂ C	0.29	0.01
W ₂ C	0.07	0.01

S3. Estimation of average equilibrium constants

For CH₄ adsorption, the most stable adsorption mode is always followed by N other adsorption modes (at least one) on different sites or/and with different orientations, which are close in energy.

Therefore, the macroscopic $K_{CH_4}(T,p)$ is likely superimposed from these contributions. We thus give an average $K_{CH_4}(T,p)$ calculated as

$$K_{CH_4}(T,p) = \sum_{j=1}^N \frac{1}{N} (K_{CH_4}^j(T,p)) \quad (3)$$

where $K_{CH_4}^j(T,p)$ is the equilibrium constant for a CH_4 adsorption with adsorption mode j . The specific adsorption modes included for each MXene are marked in bold in Tables S2-S4.

S4. CH₄ adsorption modes and energies

To distinguish the CH₄ adsorption sites on the MXene surface, we use a coordination notation, firstly pointing out the number n of atoms linked to the surface (η^n -CH₄), which depends on the orientation of the adsorbed CH₄ molecule, followed then by the number m of MXene surface metal atoms involved (μ^m) involved in the molecular adsorption, finally followed by a specification of the location of the n -contacting molecule atoms —T, B, C, or M which correspond to metal Top, metal-metal Bridge, Carbon hollow, or Metal hollow positions, respectively. For instance, η^3 -CH₄- μ^1 -C_TH_MH_C indicates that CH₄ has three atoms connected to the surface —one C and two H atoms, η^3 -CH₄— with a single surface metal atom involved (μ^1), in such a way that the CH₄ C atom is located on a metal Top site (C_T), one H is located over a Metal hollow site (H_M) and the other H is located on a Carbon hollow site (H_C). For η^1 -CH₄ adsorption modes, the location of the other three H atoms is also indicated in parenthesis to distinguish among different orientations, which allows unequivocally defining the site with the latter notations, see Figure S1.

Figure S1. Top views of the 24 different adsorption modes of CH₄ on MXenes. C_{CO₂}, C_{MXene} and H atoms by grey, brown and white spheres, respectively, and metal atoms by dark (top) or light (bottom) blue spheres.

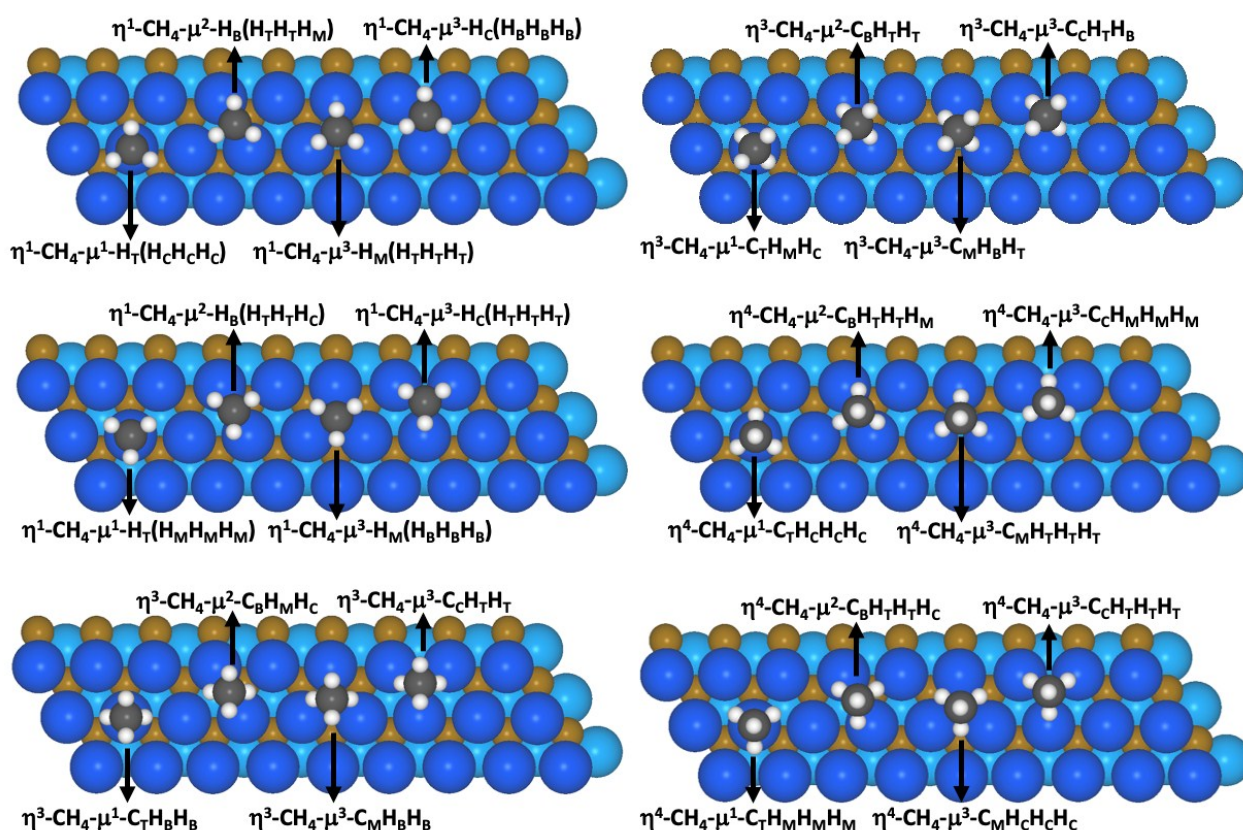


Table S2. Calculated $E_{ads}^{CH_4}$ (PBE-D3) including the ZPE term on Group IV MXenes. Numbers in bold correspond to most favorable adsorption modes for each MXene, included in the calculation of $K_{CH_4}(T,p)$. In few cases, during the geometry optimization, the initial adsorption mode moved to the reported one.

Adsorption mode	$E_{ads}^{CH_4}$ (eV)		
	Ti ₂ C	Zr ₂ C	Hf ₂ C
H _T (H _M H _M H _M)	-0.156	η^3 -CH ₄ - μ^1 -C _T H _B H _B	η^3 -CH ₄ - μ^1 -C _T H _M H _C
H _T (H _C H _C H _C)	-0.154	η^3 -CH ₄ - μ^1 -C _T H _M H _C	η^3 -CH ₄ - μ^1 -C _T H _M H _C
H _B (H _T H _T H _C)	-0.152	-0.113	-0.099
H _B (H _T H _T H _M)	-0.153	-0.109	η^4 -CH ₄ - μ^2 -C _B H _T H _T H _M
H _M (H _B H _B H _B)	-0.154	-0.111	-0.108
H _M (H _T H _T H _T)	-0.152	-0.130	-0.103
H _C (H _T H _T H _T)	-0.154	-0.133	-0.107
H _C (H _B H _B H _B)	-0.152	-0.132	-0.103
C _T H _M H _C	-0.251	-0.206	-0.129
C _T H _B H _B	-0.248	-0.202	-0.129
C _B H _T H _T	-0.176	-0.146	-0.109
C _B H _M H _C	-0.168	-0.143	-0.109
C _M H _B H _T	-0.172	C _M H _C H _C H _C	C _M H _C H _C H _C
C _M H _B H _B	C _M H _C H _C H _C	C _M H _C H _C H _C	C _M H _C H _C H _C
C _C H _T H _B	-0.186	C _C H _M H _M H _M	C _C H _M H _M H _M
C _C H _T H _T	C _C H _M H _M H _M	C _C H _M H _M H _M	C _M H _C H _C H _C
C _T H _M H _M H _M	-0.207	-0.177	-0.126
C _T H _C H _C H _C	-0.201	-0.177	-0.128
C _B H _T H _T H _C	-0.186	-0.154	-0.123
C _B H _T H _T H _M	-0.175	-0.155	-0.120
C _M H _C H _C H _C	-0.181	-0.157	-0.125
C _M H _T H _T H _T	-0.170	-0.134	-0.112
C _C H _T H _T H _T	-0.172	-0.139	-0.112
C _C H _M H _M H _M	-0.185	-0.157	-0.123

Table S3. Calculated $E_{ads}^{CH_4}$ (PBE-D3) including the ZPE term on Group V MXenes. Numbers in bold correspond to most favorable adsorption modes for each MXene, included in the calculation of $K_{CH_4}(T,p)$. In few cases, during the geometry optimization, the initial adsorption mode moved to the reported one.

Adsorption mode	$E_{ads}^{CH_4}$ (eV)		
	V ₂ C	Nb ₂ C	Ta ₂ C
H _T (H _M H _M H _M)	C _T H _M H _C	C _T H _M H _C	C _T H _M H _C
H _T (H _C H _C H _C)	C _T H _M H _C	C _T H _M H _C	C _T H _M H _C
H _B (H _T H _T H _C)	C _T H _M H _C	C _B H _T H _T H _M	C _T H _M H _C
H _B (H _T H _T H _M)	C _B H _T H _T H _M	C _B H _T H _T H _M	C _B H _T H _T H _M
H _M (H _B H _B H _B)	-0.164	-0.112	-0.140
H _M (H _T H _T H _T)	-0.169	-0.114	-0.141
H _C (H _T H _T H _T)	-0.173	-0.122	-0.147
H _C (H _B H _B H _B)	-0.163	-0.114	-0.141
C _T H _M H _C	-0.354	-0.242	-0.248
C _T H _B H _B	-0.348	-0.242	-0.242
C _B H _T H _T	C _T H _M H _C	C _B H _T H _T H _M	C _B H _M H _C
C _B H _M H _C	C _T H _M H _C	-0.123	C _T H _M H _C
C _M H _B H _T	C _M H _C H _C H _C	C _M H _C H _C H _C	C _M H _C H _C H _C
C _M H _B H _B	C _M H _C H _C H _C	C _M H _C H _C H _C	C _M H _C H _C H _C
C _C H _T H _B	C _C H _M H _M H _M	C _C H _M H _M H _M	C _C H _M H _M H _M
C _C H _T H _T	C _T H _M H _C	C _C H _M H _M H _M	C _C H _M H _M H _M
C _T H _M H _M H _M	C _T H _M H _C	C _T H _M H _C	C _T H _M H _C
C _T H _C H _C H _C	C _T H _B H _B	C _T H _B H _B	C _T H _B H _B
C _B H _T H _T H _C	-0.212	-0.139	-0.169
C _B H _T H _T H _M	-0.207	-0.142	-0.170
C _M H _C H _C H _C	-0.207	-0.138	-0.169
C _M H _T H _T H _T	-0.193	-0.126	-0.164
C _C H _T H _T H _T	-0.193	-0.126	-0.166
C _C H _M H _M H _M	-0.210	-0.143	-0.180

Table S4. Calculated $E_{ads}^{CH_4}$ (PBE-D3) including the ZPE term on Group VI MXenes. Numbers in bold correspond to most favorable adsorption modes for each MXene, included in the calculation of $K_{CH_4}(T,p)$. In few cases, during the geometry optimization, the initial adsorption mode moved to the reported one.

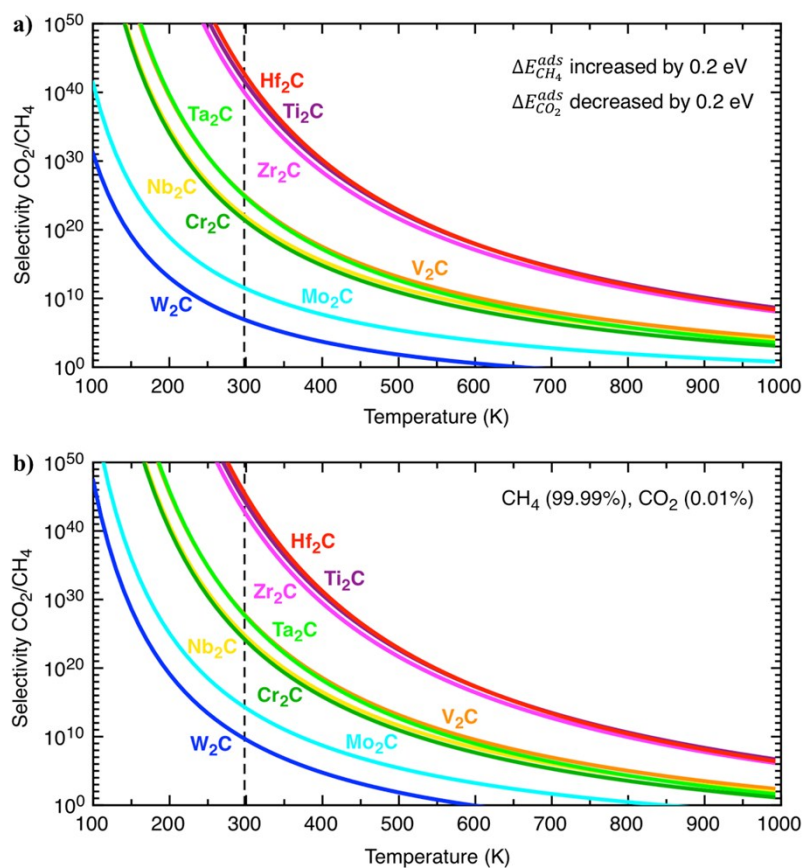
Adsorption mode	$E_{ads}^{CH_4}$ (eV)		
	Cr ₂ C	Mo ₂ C	W ₂ C
H _T (H _M H _M H _M)	-0.133	C _T H _M H _C	-0.233
H _T (H _C H _C H _C)	-0.132	C _T H _M H _C	-0.224
H _B (H _T H _T H _C)	-0.023	-0.118	-0.153
H _B (H _T H _T H _M)	-0.106	C _T H _B H _B	C _B H _T H _T H _M
H _M (H _B H _B H _B)	-0.103	-0.112	-0.155
H _M (H _T H _T H _T)	-0.085	-0.114	-0.155
H _C (H _T H _T H _T)	-0.111	-0.112	-0.152
H _C (H _B H _B H _B)	-0.108	-0.106	-0.146
C _T H _M H _C	-0.314	-0.377	H _T (H _M H _M H _M)
C _T H _B H _B	-0.253	-0.377	H _T (H _M H _M H _M)
C _B H _T H _T	-0.123	C _T H _B H _B	H _T (H _M H _M H _M)
C _B H _M H _C	-0.074	-0.130	H _T (H _M H _M H _M)
C _M H _B H _T	-0.117	C _B H _T H _T H _M	H _T (H _M H _M H _M)
C _M H _B H _B	C _M H _C H _C H _C	C _M H _C H _C H _C	C _M H _C H _C H _C
C _C H _T H _B	-0.071	C _T H _B H _B	C _C H _M H _M H _M
C _C H _T H _T	C _C H _M H _M H _M	C _C H _M H _M H _M	C _C H _M H _M H _M
C _T H _M H _M H _M	C _T H _M H _C	C _T H _M H _C	H _T (H _M H _M H _M)
C _T H _C H _C H _C	-0.129	C _T H _M H _C	H _T (H _M H _M H _M)
C _B H _T H _T H _C	-0.120	C _T H _M H _C	-0.188
C _B H _T H _T H _M	-0.119	-0.139	-0.193
C _M H _C H _C H _C	-0.126	-0.135	-0.189
C _M H _T H _T H _T	-0.120	-0.131	-0.192
C _C H _T H _T H _T	-0.035	-0.136	-0.186
C _C H _M H _M H _M	-0.029	-0.136	-0.184

S5. Lowest selectivity limit

Playing the advocate devils game, one can argue that the presently estimated ideal selectivity values might be overestimated due to a possible overbinding for CO₂ and underbinding for CH₄ on MXenes by PBE-D3, even though this has not been reported in the literature. However, it is known that standard GGA functionals may present errors of up to 0.20 eV in the adsorption energies. Therefore, we have recalculated the selectivity values for all nine MXenes by increasing $E_{ads}^{CH_4}$ by 0.2 eV and decreasing $E_{ads}^{CO_2}$ by 0.2 eV, which accounts for a lower limit. The results are reported in Figure S2a, which shows a decrease of 7 and 4 orders of magnitude in the CO₂/CH₄ selectivity at 300 and 600 K, respectively, compared to the results reported in Figure 2a of the main text. Even in this hypothetically detrimental situation, these materials still present ultra-high selectivity values, surpassing all other previously reported materials.

Furthermore, we have estimated the effect of the CO₂ molar fraction in the binary mixture. Note that the ideal selectivity calculated by means of Eq. 1 does not depend on the total pressure of the system, but it rather depends on the temperature and the partial pressures of both components — *i.e.* the CO₂ molar fraction, insomuch the smaller the CO₂ content in the binary mixture is, the lower is the selectivity. Figure S2b shows the calculated ideal selectivity values for all nine MXenes for a mixture containing 99.99% of CH₄ and 0.01% of CO₂, this is, four orders of magnitude lower than the equimolecular mixture shown in Figure 2a. This extreme situation reveals the CO₂ capture capabilities, as selectivities drop by 3-5 orders of magnitude at 300 K, but still over 10¹⁰, which translates in a purification of the CH₄ stream over 99.99%. Only in the W₂C this capability reverses at 600 K. Thus, generally, MXenes can be used for high-purity CO₂ capture even in low-CO₂ content CH₄/CO₂ mixtures, and so for CH₄ biogas upgrade up to analytical purity.

Figure S2. (a) Calculated ideal selectivity values for CO₂ over CH₄ on all nine MXenes as a function of the temperature by increasing $E_{ads}^{CH_4}$ by 0.2 eV and decreasing $E_{ads}^{CO_2}$ by 0.2 eV, or (b) considering a mixture containing 99.99% of CH₄ and 0.01% of CO₂. Grey dashed vertical lines highlight the ambient temperature of $T \sim 298$ K. Note that the ideal selectivity depends on the temperature and the partial pressures of both gases —*i.e.* mixture composition— but is independent of the total pressure.



References

- ¹ P. E. Blöchl, *Phys. Rev. B*, 1994, **50**, 17953.
- ² G. Kresse and D. Joubert, *Phys. Rev. B*, 1999, **59**, 1758.
- ³ L. H. Sprowl, C. T. Campbell and L. Árnadóttir, *J. Phys. Chem. C*, 2016, **120**, 9719.
- ⁴ G. Henkelman, B. P. Uberuaga and H. Jónsson, *J. Chem. Phys.*, 2000, **113**, 9901.
- ⁵ A. H. Larsen, J. J. Mortensen, J. Blomqvist, I. E. Castelli, R. Christensen, M. Dułak, J. Friis, M. N. Groves, B. Hammer, C. Hargus, E. D. Hermes, P. C. Jennings, P. B. Jensen, J. Kermode, J. R. Kitchin, E. L. Kolsbjerg, J. Kubal, K. Kaasbjerg, S. Lysgaard, J. B. Maronsson, T. Maxson, T. Olsen, L. Pastewka, A. Peterson, C. Rostgaard, J. Schiøtz, O. Schütt, M. Strange, K. S. Thygesen, T. Vegge, L. Vilhelmsen, M. Walter, Z. Zeng and K. W. Jacobsen, *J. Phys. Condens. Matter*, 2017, **29**, 273002.
- ⁶ S. Smidstrup, A. Pedersen, K. Stokbro and H. Jónsson, *J. Chem. Phys.*, 2014, **140**, 214106.
- ⁷ A. Morales-García, A. Fernández-Fernández, F. Viñes and F. Illas, *J. Mater. Chem. A*, 2018, **6**, 3381.